Rev. Adv. Mater. Sci. 48 (2017) 52-61

LATTICE EXPANSION AND GRAIN BOUNDARY EXCESS VOLUME OF NANOCRYSTALLINE Se PREPARED BY MECHANICAL MILLING

Y.H. Zhao[1] and Y.T. Zhu[1,2]

[1]Nano Structural Materials Center, School of Materials Science and Engineering, Nanjing University of Science and Technology, Nanjing 210094, China
[2]Department of Materials Science & Engineering, North Carolina State University Raleigh, NC 27695-7919, USA

Received: December 07, 2016

Abstract. Lattice constant is one of the most principle crystal parameters, which critically determines physical, chemical, mechanical and thermodynamic, and other properties. Conversely, material properties could be tuned for specific applications by tailoring the lattice constants. Practically, the lattice constants were modified by controlling surface/boundary/interface, lattice solute/defect and external conditions (e.g. temperature, stress, etc.). Literature inspections on the lattice constants of nanocrystalline (nc) materials show ambiguous results indicating either lattice contraction or expansion. To clarify the contradictory results, in this work, nc Se specimens with different grain sizes were prepared by mechanical milling. Quantitative x-ray-diffraction measurements revealed that the nc Se specimens exhibit large lattice expansions with decreasing grain size. The measured lattice expansion in nc Se can be understood on the basis of the stress field generated at grain boundary (GB) due to the excess GB free volume. The measured unit cell volumes of nc Se were well fitted using a GB stress field model from which the excess GB volume also shows processing method dependence.

1. INTRODUCTION

Lattice constant/parameter is one of the most principle crystal parameters because it critically governs physical (e.g., electronic, magnetic, optical, thermal, etc.,), chemical (e.g., catalytic, cohesive, etc.), mechanical (e.g., modulus of elasticity, etc.) and thermodynamic (e.g., phase instability, stacking fault energy, etc.), etc. properties [1-15]. Conversely, by tailoring the lattice constant materials scientists can control or alter the above properties to satisfy industrial application requirements. First, examples for physical behavior altered by lattice constant, it has been reported the lattice expansion of ternary Cu_3NMg_x, realized by altering atomic percent of Mg via RF reactive magnetron co-sputtering, caused a steadily narrowed band gap that the room temperature electrical resistivity drops by four orders of magnitude [1]. For topological band structured $InAs_xSb_{1-x}$ (x = 0, 0.25, 0.5, 0.75, 1) alloys which are in a topologically trivial phase, reasonable hydrostatic lattice expansion could make them convert to nontrivial topological semiconductors with zero band gap [2]. Moreover, lattice ex-

Corresponding author: Y.H. Zhao, e-mail: yhzhao@njust.edu.cn

pansions of α-Fe and VO_2 thin films with thicknesses in nanometer scale were reported to increase magnetic moments and to suppress metal-to-insulator transition, respectively [3,4]. Second, for chemical property modified by lattice constant, cohesive energies of nanocrystalline (nc) materials, modeled using a hard-sphere approach [5], are found to increase with lattice expansion. Third, for thermodynamic behavior, first-principle calculations based on density functional theory indicate that stacking fault energy in fcc Fe increases with thermal lattice expansion [6], and phase instability occurred in bulk ceria (CeO_2) with lattice expansion [7]. In addition, experiments also reveal that lattice expansions of Si [8,9], Ge [10] and Se [11-13] can induce crystal-to-amorphous phase transformation, i.e., solid state amorphization (SSA) [14]. Finally, for mechanical properties, physical modeling shows the lattice expansion leads to a bond weakening and a suppression in Young's modulus of nc materials, while lattice contraction results in the reinforced bonding strength and an enhancement in Young's modulus of nanoparticles [15].

The equilibrium lattice constant is controlled by a local balance between short-range repulsive and long-range Coulomb forces. Practically, the lattice constant can be modified by controlling the following several factors as surface/boundary/interface, lattice solute/defect and external conditions (e.g. temperature, stress, excitation, impact ionization, etc.) [9-32]. For surface influence, based on the Gibbs–Thomson effect, lattice contraction is expected in the presence of surface curvature pressure [16]. In literature, lattice contraction was frequently observed in isolated nano-particles due to surface stress [17], which induces more hydrostatic compression on the nanoparticle as compared to micron-size particles. The change in the unit cell volume ΔV^{uc} can be expressed as:

$$\frac{\Delta V^{uc}}{V_0^{uc}} = -\frac{4\sigma}{KD}, \qquad (1)$$

where V_0^{uc} is the coarse-grained unit cell volume, σ is the surface energy, K is the bulk modulus and D is the spherical particle diameter. In contrast to the lattice contraction in nano-particles, lattice expansion was usually found in bulk nc materials consisting of nanometer-sized crystallites and a large volume fraction of grain boundaries (GBs) [18-21]. For instance, lattice expansions were reported in nc Fe_2B [22], Ni_3P [23], Se [24,25] (produced by nanocrystallization of amorphous solids, NAS), Si [8,9], Ge [10], Nb_3Sn [26], Fe, Cu [27-30] (by mechanical milling, MM), Cu by electro-deposition (ED) [28], TiO_2 [31] (by sol-gel method), Cr by inert gas condensation (IGC) [32]. It is interesting that the lattice contraction of ZrO_2 nano-powders was transformed to the lattice expansion of bulk nc ZrO_2 during spark plasma sintering (SPS) [33,34]. The lattice expansion in nc materials reflects GB effect on the lattice constant. Interfacial effect on the lattice constant was reported during nitriding of iron-based alloys in which the development of mis-fitting coherent nitride precipitates in a ferrite matrix induces an overall expansion of the ferrite lattice [35]. Both substantial/interstitial solute atoms and point defects (e.g., vacancies) can change the lattice constant via their different atom sizes from that of the solvent matrix. Lattice expansions in both free-standing Al and W-1%Re alloy foils are induced by irradiation with MeV-energy heavy projectiles (C, O, Si, and He ions) [36,37]. In literature [38], the authors found the lattice constant changes in nanostructured TiO_2 wires depends systematically on the relative concentration and type of defects such as oxygen vacancies and Ti interstitials. During aging of 7075 Al alloys, we also observed a gradual decrease of lattice parameter due to the dissolution of Al matrix [39]. For external condition of stress etc. influences, lattice constant changes are observed in Ni [40], Si [41,42], Nb [43,44] Pd [45], Ge [46], Cu [47], Ti_3Al [48] thin films by sputtering deposition due to the existence of residual stress. In addition, it is reported that a tetragonal lattice expansion with enhanced elongation along the [001] crystal axis in (In,Ga)As quantum dots arises from excitation induced lattice heating [49]. Moreover, in situ atomic resolution transmission electron microscopy directly observed a highly localized anomalously large lattice expansion inside a bilayer grapheme constriction at high bias [50].

Inspection on literatures about the grain-size dependence of the lattice constant of bulk nc materials indicate that except lattice expansion as mentioned above, minor lattice contractions were also observed in nc Pd by consolidation of ultrafine nanoparticles [51,52], Cu by severe plastic deformation [53], W [30] by MM, Fe-C by rolling [54]. Also, some ambiguous results indicate both contraction and expansion of the lattice were observed for the same system or experiment, for instance nc Pd [52,55], disparate behavior is observed in different investigations – at smaller grain sizes <8 nm, lattice expansion was observed [55], whereas for grain sizes >8 nm, lattice contraction was reported [52]. This hints at specific grain-size regimes for the occurrence of

expansion or contraction. Recently, Mittimeijer et al. [30,56] revealed a non-monotonic variation of the lattice parameter in nc Ni and Cu prepared by MM with grain size, exhibiting contraction down to a particular critical grain size followed by a change to lattice expansion for smaller grain sizes.

The above complicated or contradictory results on the lattice constant changes in bulk nc materials might be resulted from many extraneous factors, such as impurities by MM and residual stresses induced by non-equilibrium processing. Moreover, the experimental determination of lattice constants may be affected by measurement errors, such as those associated with peak broadening and weakening, peak shifting, and non-symmetries associated with the interactions of X-rays and neutrons with nanometer-sized crystallites [57]. Hence, partly because of these experimental challenges, and partly due to conflicting results from published studies, the question whether nc materials exhibit inherent variations in lattice parameter remains mostly unanswered.

Motivated by the above question, the present study was undertaken to systematically study variations in lattice constant with grain size using tretragonal Se as a model material. Mechanical milling was employed to synthesize nc Se with varying grain sizes. Elemental Se was selected as a model material because of its special structure of helical $[\text{-Se-}]_n$ molecular chains with intra-chain covalent bonds and inter-chain Van der Waals forces. The weak Van der Waals force makes it easy for the lattice constant to change.

2. EXPERIMENTAL DETAILS

Mechanical milling of pure Se powders (with a purity of 99.999% and particle size smaller than 600 mesh) was carried out in a high-energy vibratory ball mill with stainless steel balls and vial at ambient temperature. The ball-to-powder weight ratio was 10 to 1. To avoid oxidation, about 4.5 g Se powder was charged into the vial and sealed by an elastic O-ring under dry Ar atmosphere (O_2, $H_2 < 5$ ppm) with an over-pressure of about 3 atm. Each mechanical milling procedure was started with a new batch of initial powder and was carried out without interruption. Wet chemical analysis and energy-dispersive X-ray analysis indicated that the O content was less than 0.1 wt.% and the Fe content less than 0.02 wt.% in the sample milled for 30 min.

Quantitative X-ray diffraction (XRD) measurements of the different grain-sized nc-Se samples were carried out on a Rigaku D/MAX 2400 X-ray diffractometer with a wide angle goniometer. The milled nc-Se powders used for XRD measurements were filled in the groove of the XRD specimen holder. A rotating Cu target was used with a voltage of 50 kV and a current of 100 mA to increase the diffraction peak intensity. The X-ray wavelengths λ_{ka1}(=1.540 56 Å) and λ_{ka2} (=1.544 39 Å) were selected using a graphite crystal <0002> scattering at the goniometer receiving slit section. With these wavelengths, the extinction depth in Se was calculated to be less than 87 μm, which was much smaller than the thickness of the measured sample. The divergence slit (which was placed in the incident X-ray beam) was selected with a width of 0.5, ensuring that the entire beam is either absorbed or diffracted by the sample. The scattering slit (which controls the scattering X-ray on the counter) was also chosen with a width of 0.5°. The width of 0.15 mm was selected as that of the receiving slit (which controls the width of diffracted X-ray to be entered into the counter). Measurements of θ-2θ scans for the samples were made in the reflection mode with the scattering vector aligned approximately perpendicular to the sample surface. The experimental temperature was 293K and the scan range for 2θ was 20°–103°. A small angular step of 2θ (0.02°) and a fixed counting time of 10 s were taken to measure the intensity of the Bragg reflections. For the rest of the XRD pattern, which is related to the background intensity, a step size of 0.1° and a counting time of 5 s were used.

3. RESULTS

3.1. Grain size and microstrain

Fig. 1 shows typical XRD patterns for milled nc Se samples with different milling times. The nc Se samples prepared by mechanical milling have a tetragonal structure. It is obvious that with an increase in milling time, the Bragg diffraction lines are significantly broadened, and the peak positions shift towards lower 2θ values, suggesting a lattice expansion. To calculate grain size, microstrain and lattice parameters, the XRD Bragg diffraction lines are fitted by using the Pseudo-Voigt function [57,58] from which the Lorentzian and Gaussian fractions, integral width and peak position could be obtained. Detailed fitting process was described in Ref. 25.

The grain size of the nc Se samples was calculated on the basis of an XRD peak broadening method. The peak broadening is characterized by its integral width. The measured intensity profile of the Bragg reflection is a convolution of the physical

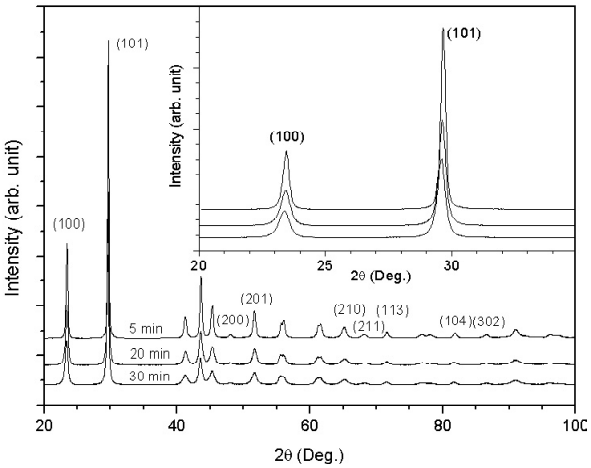

Fig. 1. The X-ray diffraction patterns of the nc Se samples with different milling time.

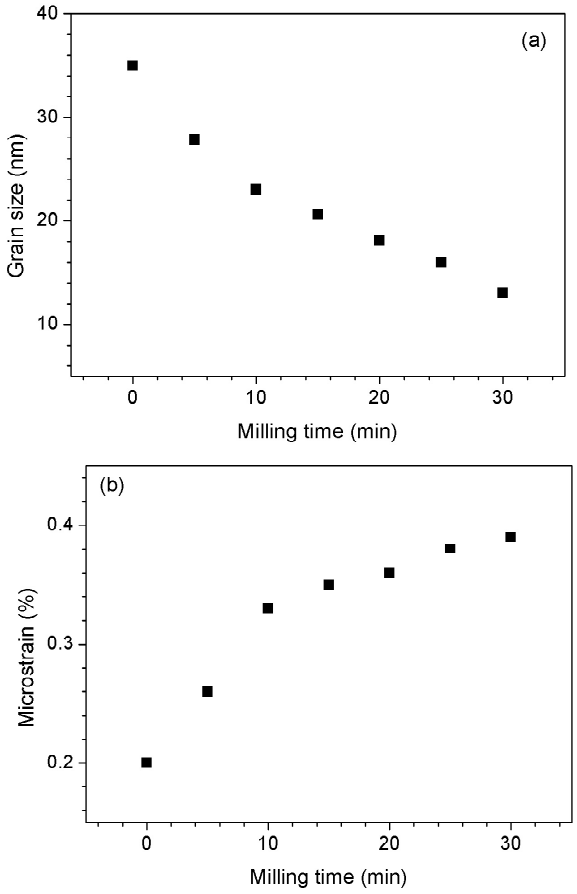

Fig. 2. Milling time dependences of grain size and microstrain.

intensity profile from the sample with a profile representing instrumental broadening. The measured profile of the Bragg reflection in the nc-Se sample possesses primarily a Lorentzian component [25]. The instrumental broadening profile determined by means of a SiO_2 reference sample is revealed as to be a Gaussian type [25]. So, one can suppose that the physical profile of the nc Se is primarily a Lorentzian type. Therefore, one can separate the physical intensity profile from the measured intensity profile by removing the instrumental broadening effect. The microstructure broadening of the sample may originate from impurities, small crystallites, and the presence of microstrain within the specimen. As the effect of impurities can be ruled out for the pure nc-Se samples in this case, the physical broadening profile can be considered as the convolution of the grain-size broadening profile (usually represented by a Lorentzian function [57]) with that of the microstrain broadening (a Gaussian function [59]). Then the grain size and the microstrain of the sample can be calculated from the integral width of the physical broadening profile in terms of the Scherrer and Wilson equation [59]:

$$\frac{\beta_{hkl}^2}{tg^2\theta_{hkl}} = \frac{\lambda\beta_{hkl}}{D_{hkl}tg\theta_{hkl}\sin\theta_{hkl}} + 16 < \varepsilon_{hkl}^2 >^{1/2}, \qquad (2)$$

where λ is the wavelength of Cu $K_{\alpha 1}$ irradiation, D_{hkl} and $<\varepsilon_{hkl}>^{1/2}$ represent the thickness and the mean magnitude of microstrain of the grains in the *<hkl>* direction, respectively. By performing a least-square fit to $\beta^2_{hkl}/tg^2\theta_{hkl}$ plotted against $\lambda\beta_{hkl}/(tg\theta_{hkl}\sin\theta_{hkl})$ for all of the measured peaks of the samples, we are able to determine the mean grain size *D* and the mean microstrain $<\varepsilon^2>^{1/2}$. Standard linear regression techniques provide an estimate for the uncertainty in the parameters from the error in the fit [60].

The calculated grain size and microstrain of the milled nc Se samples versus mechanical milling time are shown in Fig. 2 and listed in Table 1. With increasing milling time, the grain size decreased gradually from 35 to 13 nm, and the microstrain increased from 0.2 to 0.39%. The microstrain value is smaller than that of nc Se prepared by NAS (0.8%) [25].

3.2. Lattice parameter and unit cell volume

Determination of the lattice parameters in nc Se includes two stages. First, the λ_{ka2} component was removed from the XRD profiles using the modified Rachinger method [61,62] Second, the lattice parameters were calculated from the intensity peak centroid positions for the nc-Se specimens. The peak positions were calibrated by the external stan-

Table 1. A list of grain size *D*, microstrain $<\varepsilon^2>^{1/2}$, lattice parameters *a*, *c* and unit cell volume *V* of the nc Se by mechanical milling. The *D*, $<\varepsilon^2>^{1/2}$, *a*, *c* measurement errors are ±2 nm, ±0.02%, ±0.001 Å and ±0.001 Å.

Milling time (min)	*D* (nm)	$<\varepsilon^2>^{1/2}$ (%)	*a* (Å)	*c* (Å)	*V* (Å^3)
0	35	0.20	4.3660	4.9580	81.84731
5	28	0.26	4.3666	4.9573	81.85825
10	23	0.33	4.3664	4.9574	81.85240
15	21	0.35	4.3666	4.9567	81.84834
20	18	0.36	4.3669	4.9560	81.84803
25	17	0.38	4.3679	4.9549	81.86734
30	13	0.39	4.3702	4.9564	81.96427

dard method using a pure Si polycrystal in order to minimize the system error. The calibration function was observed as:

$$\Delta 2\theta = \alpha + \beta\cos\theta + \gamma\sin\theta, \quad (3)$$

where α relates to 2θ-axis origin displacement, β relates to eccentricity between the sample and goniometer center axis, and γ relates to the sample flatness or absorption. In this study, α, β, and γ were determined by the least-square method, being 0.013 891, -0.080 571, and 0.023 696, respectively. Considering that the nc Se is the tetragonal structure, we select the weighted least-square method to calculate the lattice parameters in order to minimize the calculation error. The equation is originated from the Bragg's law and given by

$$\frac{h^2a^*}{2}+\frac{k^2b^*}{2}+\frac{l^2c^*}{2}+\frac{2klb^*c^*}{\cos\alpha^*}+ \frac{2lha^*c^*}{\cos\beta^*}+\frac{2hka^*b^*}{\cos\gamma^*}+E(\theta)x=\frac{4\sin^2\theta}{\lambda^2}, \quad (4)$$

where *a**, *b**, *c** and α^*, β^*, γ^* are the reciprocal-lattice parameters from which the lattice parameters of the nc Se can be obtained. *E(θ)* is the error function that is selected as $\sin^2 2\theta$ and *x* is the error function weight. The values of the lattice parameters of the nc Se were finally calculated from the intensity centroid positions of nine single peaks (100), (101), (200), (201), (210), (211), (113), (104) and (302).

The measured *a* and *c* for the nc Se samples with varying grain size, *D*, were shown in Figs. 3a and 3b and listed in Table 1. For comparison, the *a* and *c* values of the nc Se by NAS were also drawn in the figures. The *a* of the nc Se samples prepared by NAS and MM exhibit the similar variations against the grain size: increase with decreasing grain size. But the *a*-*D* curve of the milled nc Se is lower than that of the nc Se by NAS. The largest *a* (*D* = 13 nm, by NAS) is about 0.29 % larger than the equilibrium value a_0 (= 4.3662 Å). The *a* change against grain size is far beyond the error bar which was estimated to be about 0.001 Å. The *c* values of the milled nc Se are smaller than those of the equilibrium value c_0 (= 4.9580 Å), while *c* values of the crystallized nc Se are larger than that of the c_0. With decreasing grain size, the *c* slightly decreases. The measurement error of *c* was about 0.001 Å. With the measured *a* and *c*, the unit cell volume V^{uc}_{nc} of the nc Se

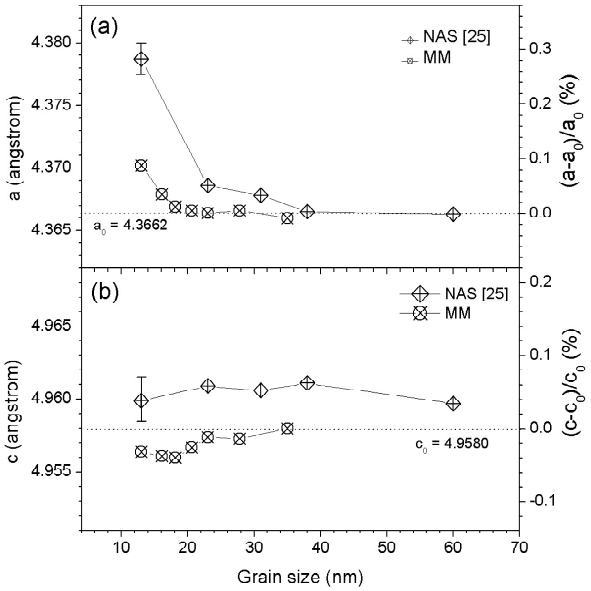

Fig. 3. The measured lattice parameters *a* (a), *c* (b), and their deviations from the corresponding equilibrium values a_0 and c_0 of the nc Se samples prepared by different synthesis methods (nano-crystallization of amorphous Se, NAS; mechanical milling, MM). The error for *a* and *c* is about 0.001 Å.

samples can be calculated according to $V_{nc}^{uc} = \left(\sqrt{3}/2\right)a^2c$, as shown in Fig. 4. The values of V_{nc}^{uc} are found to be larger than the equilibrium data (V_0^{uc} = 81.8548 Å^3) for all the nc Se specimens with small grain sizes, and increase with decreasing grain size, depending on the synthesis methodology used.

4. DISCUSSIONS

The evident lattice expansions in the nc Se samples prepared by different methods appeared to be an intrinsic nature of nc Se materials, although the expansion amplitudes of the lattice constants are dependent on the synthesis method used. To understand the lattice expansion phenomena, several models/approaches were proposed in literature involving the effect of intra-crystalline pressure [63], interface stress [64,65], excess GB volume [66-70] and supersaturation of vacancies [71].

4.1. Thermodynamic super-saturation model

From a thermodynamic consideration, the solubility of a solution will be increased significantly when the grain size is in the nanometer regime due to its higher energetic state [71], indicating that a supersaturated solution structure might be expected in nanocrystallites. The enhanced solubility can be expressed as the Gibbs-Thomson equation:

$$C(T,D) = \frac{4\gamma\Omega C_0}{kTD}, \quad (5)$$

where C_0 is the equilibrium solute stability in the coarse-grained crystal, k is the Boltzmann constant, γ is the interfacial free energy, Ω is the atomic volume and D the grain size. In a pure system or in a stoichiometric intermetallic compound, the only possible 'solute atom' is either point defects or vacancies. Similarly, an increase in the solubility of the point defects or vacancies in nanocrystallites can also be expected. In nc pure metals, the equilibrium concentration of vacancies will be increased by

$$C^v(T,D) = \frac{4\Omega\gamma\, exp(\frac{S_f^v}{k}) exp(\frac{-E_f^v}{kT})}{kTD}, \quad (6)$$

where S^v_f and E^v_f are the formation entropy and formation energy for the vacancy, respectively. Therefore, the deviation from the perfect crystal lattice in nc system can be ascribed to a super-saturation of vacancies inside the nanocrystallites. The solution of vacancies in the crystal lattice will disturb the atomic arrangement around the vacancies to some extent, and ultimately results in an expanded lattice structure. The smaller the grain size, the higher the concentration of vacancies, i.e., the more significant will be the resultant lattice expansion.

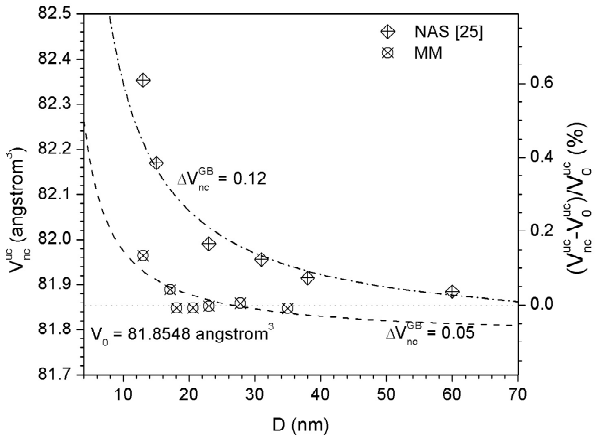

Fig. 4. The unit cell volume V_{nc}^{uc} and its deviation from the equilibrium value V_0^{uc} versus the mean grain size in the nc Se specimens prepared by different synthesis methods (nanocrystallization of amorphous Se, NAS; mechanical milling, MM). The dashed lines are the fitted curves according to Eq. (11) from which the excess GB volumes are 0.05 and 0.12 for NAS and MM prepared nc Se.

4.2. GB stress model and GB excess volume

The GB stress model based on the GB excess volume ΔV_{nc}^{GB} was proposed under the fact that the nc materials possess large volume fraction of GBs, implying an increased GB-to-volume ratio: the GB volume fraction is almost 50% at a grain size of 2.5 nm [72]. Several studies indicate that ΔV_{nc}^{GB} contained in the GBs of nc materials is of cardinal importance for their properties [73]. Accordingly, nc materials are considered to be inherently heterogeneous, composed of ordered crystallites embedded in a framework of highly disordered GBs [74,75]. Several experimental studies revealed the presence of vacancies in excess and vacancy clusters/voids [66,67,76–78] and a highly disordered structure at GBs [74] for nc materials. These defects, as structural elements of nc materials, together with the geometrical constraints to the GB structure give rise

to the notion of ΔV_{nc}^{GB} [79]. The ΔV_{nc}^{GB} generates displacement fields and thus induces distortion of the surrounding crystal lattices [80-82]. A vacancy induces a radial displacement field characterized by displacements of the neighbouring atoms towards the vacancy [83, 84].

On the above basis, a model for the stress field generated by ΔV_{nc}^{GB} was developed by Qin et al. [66-68]. Because the density of the GBs is far less than that of perfect crystallites, the ΔV_{nc}^{GB} is defined as

$$\Delta V_{nc}^{GB} = \frac{V_{nc}^{GB} - V_0^{pc}}{V_0^{pc}}, \quad (7)$$

where V_{nc}^{GB} and V_0^{pc} are the molar volumes of the GBs and the perfect crystallites, respectively. The vacancies in excess and vacancy clusters/voids [66,67,76–78] at GBs will induce a stress field which diminish according to $1/x^3$ [85,86], where x is the distance to the center of the defects at GBs. Under the effects of the stresses, the atoms in the nanocrystallites will deviate from their equilibrium sites, resulting in lattice distortion. According to the theory of elasticity [86] the displacement of an atom from its normal site will obey $1/x^2$. Therefore, the relative displacement of two adjacent atoms in the crystallite is estimated to be proportional to $(1/x^2)$-$(1/(x+r_0)^2)$, where r and r_0 are the nearest-neighbor distance of a distorted and a perfect lattice. A nc polycrystal consisting of square-shaped crystallites with orthogonal GB systems, where the atoms in the crystallites are simultaneously under the influence of the surrounding stress field, was considered. By assuming the GB structure is approximated by a dilated crystal, the mean value $(\sqrt[3]{1+\Delta V_{nc}^{GB}}-1)r_0$ can be used as a substitute for the relative displacement of two adjacent atoms at GBs. So the total relative displacements of two adjacent atoms, Δr, in the crystallites and at GBs are given by

$$\Delta r = A\left[\frac{1}{x^2} - \frac{1}{(x+r_0)^2} + \frac{1}{(D+\xi-x)^2} - \frac{1}{(D+\xi-x+r_0)^2}\right], \quad \frac{\xi}{2} < x < D+\frac{\xi}{2}, \quad (8)$$

$$\Delta r = (\sqrt[3]{1+\Delta V_{GB}}-1)r_0, 0 \le x < \frac{\xi}{2}, \quad (9)$$

where ξ is the mean width of the GBs, D is the mean grain size and A is a correlation coefficient. The mean value of $\overline{\Delta r}$ in the entire grain can be given by

$$\overline{\Delta r} = \frac{r_0}{2D}\frac{\xi(\xi+2r_0)}{\xi+r_0}(\sqrt[3]{1+\Delta V_{nc}^{GB}}-1), \quad (10)$$

With respect to f.c.c. crystals, $\frac{\overline{\Delta r}}{r_0}$ is equal to $\frac{\overline{\Delta a}}{a_0}$ (= $\frac{a-a_0}{a_0}$), where a is the mean lattice parameter of a distorted crystallite. The unit cell volume expansion V_{nc}^{uc} can be expressed as follows:

$$\Delta V_{nc}^{uc} = \frac{V_{nc}^{uc} - V_0^{uc}}{V_0^{uc}} \approx \frac{3(r-r_0)}{r_0} = \frac{3}{2D}\frac{\xi(\xi+2r_0)}{\xi+r_0}(\sqrt[3]{1+\Delta V_{nc}^{GB}}-1), \quad (11)$$

The GB width is usually equal to 1 nm [5, 68-70], and r_0 is equal to 2.373 Å for coarse-grained Se. The ΔV_{nc}^{GB} can be calculated by fitting the experimentally measured V_{nc}^{uc} values using Eq. (11), as plotted in dashed lines in Fig. 4. The ΔV_{nc}^{GB} of nc Se prepared by NAS and MM methods are 0.12 and 0.05, respectively. A larger ΔV_{nc}^{GB} corresponds to a more disordered GB structure and a higher GB enthalpy. The different GB structures of the nc Se samples can be understood qualitatively from their synthesis methods. The nanocrystallization of amorphous Se is accompanied by a large volume shrinking process, which generates large amount of vacancies and/or vacancy clusters at GBs [66,67]. The grain refinement process of crystalline Se by the MM method does not introduce a volume shrinkage, and therefore corresponds to the smallest ΔV_{nc}^{GB}.

5. CONCLUSIONS

In summary, this paper reviewed the previous results on lattice parameter changes in bulk nc materials, both lattice expansion and contraction were reported in literature. Then by quantitative XRD measurements we revealed that the lattice constants of nc Se increase with decreasing grain size. This phenomenon occurred in nc Se prepared by mechanical milling of crystalline Se and nano-crystallization of amorphous Se, suggesting that the lattice expansion in nc Se is intrinsic. The magnitude of lattice expansion depends on the processing method, because the GB structure is affected by the way these GBs were created (i.e. the processing method). In the discussion part, we reviewed the models of GB stress and supersaturated va-

cancy for the lattice expansion, and used the GB stress field model to satisfactorily fit the grain-size dependence of the lattice constants. The excess GB volume from the fitting results also shows processing method dependence.

ACKNOWLEDGEMENTS

The authors would like to acknowledge support by National Natural Science Foundation of China (51225102 and 2012CB932203), The 8th"Liu Da Ren Cai Gao Feng B932203) from Jiangsu Province, China, and the Jiangsu Key Laboratory of Advanced Nanomaterials and Technologies.

REFERENCES

[1] T. Xu, Z.X. Cao and A.L. Ji // *Journal of Alloys and Compounds* **685** (2016) 423.
[2] S. Namjooa, A.S.H. Rozatian and I. Jabbari // *Journal of Alloys and Compounds* **628** (2015) 458.
[3] I. Dirba, P. Komissinskiy, O. Gutfleisch and L. Alff // *Journal of applied physics* **117**, (2015) 173911.
[4] D. Passarello, J. Jeong, M. G. Samant and S. S. P. Parkin // *Applied Physics Letters* **107** (2015) 201906.
[5] Y. F. Zhu, W. T. Zheng and Q. Jiang // *Applied Physics Letters* **95**, (2009) 083110.
[6] V. I. Razumovskiy, A. R. Huamantinco, P. Puschnig and A. V. Ruban // *Physical Review B* **93** (2016) 054111.
[7] J. Buckeridge, D. O. Scanlon, A. Walsh, C. R. A. Catlow and A. A. Sokol, // *Physical Review B* **87** (2013) 214304.
[8] E. Gaffet and M. Harmelin // *Journal of Less-Common Metals* **157** (1990) 201.
[9] T. D. Shen, C. C. Koch, T. L. Mccormick, R. J. Nemanich, J. Y. Huang and J. G. Huang // *Journal of Materials Research* **10** (1995) 139.
[10] E. Gaffet // *Materials Science and Engineering A* **136** (1991) 161.
[11] Y.H. Zhao, Z.H. Jin and K. Lu // *Philosophical Magazine Letter* **79** (1999) 747.
[12] Y.H. Zhao, K. Lu and T. Liu // *Journal of Non-Crystalline Solids* **333** (2004) 246.
[13] Y.H. Zhao, Y.T. Zhu and T. Liu // *Journal of Applied Physics* **95** (2004) 7674.
[14] Y.H. Zhao // *Journal of Non-Crystalline Solids* **352** (2006) 5578.
[15] Y. F. Zhu, W. T. Zheng and Q. Jiang // *Physical Chemistry Chemical Physics* **13** (2011) 21328.
[16] J. W. Gibbs, *Collected Works* (Longmans, Green & Co., New York, 1928).
[17] C. Q. Sun // *Progress in Materials Science* **54** (2009) 179.
[18] H. Gleiter // *Progress in Materials Science* **33** (1989) 223.
[19] C. Suryanarayana and C.C. Koch // *Hyperfine Interacions* **130** (2000) 5.
[20] C. C. Koch, *Nanostructured Mateials – Processing, Properties and Potential Applications* (Noyes Publications/William Andrew Publishing, Norwich, New York, 2002).
[21] M. A. Meyers, A. Mishra and D. J. Benson // *Progress in Materials Science* **51** (2006) 427.
[22] X. D. Liu, K. Lu, B. Z. Ding and Z. Q. Hu // *Nanostructed Materials* **2** (1993) 581.
[23] M. L. Sui and K. Lu // *Materials Science and Engineering A* **179-180** (1994) 541.
[24] H. Y. Zhang, K. Lu and Z. Q. Hu // *Journal of Physics-Condensed Matter* **7** (1995) 5327.
[25] Y. H. Zhao, K. Zhang and K. Lu // *Physical Review B* **56** (1997) 14322.
[26] Y. S. Cho and C. C. Koch // *Materials Science and Engineering A* **141** (1991) 139.
[27] Y. H. Zhao, H. W. Sheng and K. Lu // *Acta Materialia* **49** (2001) 365.
[28] K. Lu and Y.H. Zhao // *Nanostructured Materials* **12** (1999) 559.
[29] Y. H. Zhao, K. Lu and K. Zhang // *Physical Review B* **66** (2002) 085404.
[30] G. K. Rane, U. Welzel, S. R. Meka and E. J. Mittemeijer // *Acta Materialia* **61** (2013) 4524.
[31] A. M. Tonejc, I. Djerdj and A. Tonejc // *Materials Science and Engineering C* **19** (2002) 85.
[32] J. A. Eastman and M. R. Fitzsimmons // *Journal of Applied Physics* **77** (1995) 522.
[33] E. K. Akdogan, I. Savklýyýldýz, H. Bicer, W. Paxton, F. Toksoy, Z. Zhong and T. Tsakalakos // *Journal of Applied Physics* **113** (2013) 233503.
[34] M. B. Ponnuchamy and A. S. Gandhi // *Scripta Materialia* **83** (2014) 21.
[35] M. Akhlaghi, T. Steiner, S.R. Meka, A. Leineweber and E. J. Mittemeijer // *Acta Materialia* **98** (2015) 254.
[36] H. Minagawa, H. Tsuchida, R. Murase and A. Itoh // *Nuclear Instruments and Methods in Physics Research B* **372** (2016) 38.
[37] F. Hofmann, D. Nguyen-Manh, M. R. Gilbert, C. E. Beck, J. K. Eliason, A. A. Maznev, W. Liu, D. E. J. Armstrong, K. A. Nelsond

and S. L. Dudarev // *Acta Materialia* **89** (2015) 352.
[38] B. Santara, P. K. Giri, K. Imakita and M. Fujii // *Journal of Physics-Condensed Matter* **47** (2014) 215302.
[39] Y. H. Zhao, X. Z. Liao, Z. Jin, R. Z. Valiev and Y. T. Zhu // *Acta Materialia* **52** (2004) 4589.
[40] X. D. Liu, H. Y. Zhang, K. Lu and Z.Q. Hu // *Journal of Physics-Condensed Matter* **6** (1994) L497.
[41] Y. H. Zhao, J. Y. Wang and E. J. Mittemeijer // *Thin Solid Films* 433 (2003) 82.
[42] Y.H. Zhao, J.Y. Wang and E.J. Mittemeijer // *Applied Physics A: Materials Science and Processing* **79** (2004) 681.
[43] R. Banerjee, E. A. Sperling, G. B. Thompson, H. L. Fraser, S. Bose and P. Ayyub // *Applied Physics Letters* **82** (2003) 4250.
[44] D. Hazra, S. Datta, M. Mondal, J. Ghatak, P. V. Satyam and A. K. Gupta // *Journal of Applied Physics* **103** (2008) 103535.
[45] D. R, Raghunathan and V. S. Sadhana // *Acad P. Eng. S* **28** (2003) 47.
[46] Z. M. Wang, J. Y. Wang, L. P. H. Jeurgens, F. Phillipp and E. J. Mittemeijer // *Acta Materialia* **56** (2008) 5047.
[47] J. Sheng, U. Welzel and E.J. Mittemeijer // Applied Physics Letters **97** (2010) 53109.
[48] Y.H. Zhao, U. Welzel, J. van Lier and E. J. Mittemeijer // *Thin Solid Films* **514** (2006) 110.
[49] S. Tiemeyer, M. Bombeck, H. Göhring, M. Paulus, C. Sternemann, J. Nase, F. J. Wirkert, J. Möller, T. Büning, O. H. Seeck, D. Reuter, A. D. Wieck, M. Bayer and M. Tolan // *Nanotechnology* **27** (2016) 425702.
[50] F. Borrnert, A. Barreiro, D. Wolf, M. I. Katsnelson, B. Buchner, L. M. K. Vandersypen and M. H. Rummeli // Nano Letters **12** (2012) 4455.
[51] J. A. Eastman, M. R. Fitzsimmons and L. J. Thompson // *Philosophical Magazine B* **66** (1992) 667.
[52] R. Birringer, M. Hoffmann and P. Zimmer // *Physical Review Letters* **88** (2002) 206104.
[53] K. Zhang, I. V. Alexandrov, R. Z. Valiev and K. Lu // Journal of Applied Physics **80** (1996) 5617.
[54] M. Liu, B. Shi, J. Guo, X. Cai and H. Song // *Scripta Materialia* **49** (2003) 167.
[55] R. Divakar and V. S. S. Raghunathan // *Acad. P. Eng. S.* **28** (2003) 47.
[56] J. Sheng, G. Rane, U. Welzel and E. J. Mittemeijer // *Physica E* **43** (2011) 1155.
[57] J. I. Langford, R. Delhez, Th. H. de Keijser and E. J. Mittemeijer // Australian Journal of Physics **41** (1988) 173.
[58] D. E. Cox, J. B. Hastings, L. P. Cardoso and L.W. Finger// *Materials Science Forum* **9** (1986) 1.
[59] H. P. Klug and L. E. Alexander, *X-ray Diffraction Procedures for Polycrystalline and Amorphous Materials*, 2nd ed. (John Wiley and Sons, New York, 1974).
[60] P. R. Bevington, *Data Reduction and Error Analysis for the Physical Sciences*. (McGraw-Hill, New York, 1969).
[61] J. Labell, A. Zagofsky and S. Pearman // *Journal of Applied Crystallography* **8** (1975) 499.
[62] G. Platbrood // *Journal of Applied Crystallography* **16** (1983) 24.
[63] M. Y. Gamarnik // *Phys Status Solidi B* **168** (1991) 389.
[64] J. S. Vermaak, C. W. Mays and D. Kuhlmann-Wilsdorf // *Surface Science* **12** (1968) 128.
[65] R. Birringer, M. Hoffmannv and P. Zimmer // *Physical Review Letters* **88** (2002) 206104.
[66] M. L. Sui, K. Lu and W. Deng // *Physical Review B* **44** (1991) 6466.
[67] M. L. Sui, L. Y. Xiong and W. Deng // *Journal of Applied Physics* **69** (1991) 4451.
[68] W. Qin, Z. H. Chen, P. Y. Huang and Y. H. Zhuang // *Journal of Alloys and Compounds* **292** (1999) 230.
[69] W. Qin, T. Nagase, Y. Umakoshi and J. A. Szpunar // *Journal of Physics: Condensed Matter* **19** (2007) 236217.
[70] W. Qin, T. Nagase, Y. Umakosh and J. A. Szpunar // Philosophical Magazine Letters **88** (2008) 169.
[71] K. Lu and M. L. Sui // *Journal of Materials Science and Technology* **9** (1993) 419.
[72] H. E. Schaefer, R. Wurschum, R. Birringer and H. Gleiter // *Journal of Less-Common Metals* **140** (1988) 161.
[73] H. J. Fecht // *Acta Metallurgical Materials* **38** (1990) 1927.
[74] W. Wunderlich, Y. Ishida and R. Maurer // *Scripta Metallurgical Materials* **24** (1990) 403.
[75] T. Haubold, R. Birringer, B. Lengeler and H. Gleiter // *Physical Letters A* **135** (1989) 461.

[76] Van S. Petegem, Torre F. Dalla, D. Segers and H. Van Swygenhoven // *Scripta Materialia* **48** (2003) 17.
[77] H. E. Schaefer, R. Wurschum, R. Birringer and H. Gleiter // *Physical Review B* **38** (1988) 9545.
[78] M. J. Zehetbauer, G. Steiner, E. Schafler, A. Korznikov and E. Korznikova // *Materials Science Forum* **57** (2006) 503.
[79] H. J. Fecht // *Physical Review Letters* **65** (1990) 610.
[80] B. Baretzky, M.D. Baro, G.P. Grabovetskaya, J. Gubicza, M.B. Ivanov, Yu.R. Kolobov, T.G. Langdon, J. Lendvai, A.G. Lipnitskii, A.A. Mazilkin, A.A. Nazarov, J. Nogues, I.A. Ovidko, S.G. Protasova, G.I. Raab, A. Revesz, N.V. Skiba, J. Sort, M.J. Starink, B.B. Straumal, S. Surinach, T. Ungar and A.P. Zhilyaev // *Reviews on Advanced Materials Science* **9** (2005) 45.
[81] A. A. Nazarov, A. E. Romanov and R. Z. Valiev // *Acta Metallurgical Materials* **41** (1993) 1033.
[82] W. Qin and J. A. Szpunar // *Philosophical Magazine Letters* **85** (2005) 649.
[83] Y. Ohta, M. W. Finnis, D. G. Pettifor and A. P. Sutton // *Journal of Physics F – Met Physics* **17** (1987) L273.
[84] J. D. Eshelby, In: *Vacancies'76 Proceedings*, ed. by R. E. Smallman and J. E. Harris (The Metals Society, London, 1977), p. 3.
[85] H. Kronmuller, M. Fahnle, M. Domann, H. Grimm, R. Grimm and B. Groger // *J. Magn. Magn. Mater.* **13** (1979) 53.
[86] *The Physics of Metals*, ed. by D. Feng (Scientific Press, Beijing, 1987), p. 173.